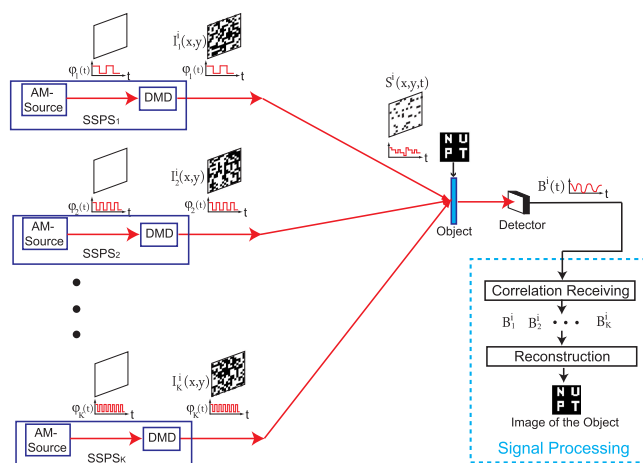


Multiple-Input Single-Output Ghost Imaging

Volume 12, Number 3, June 2020

Le Wang
Shengmei Zhao



DOI: 10.1109/JPHOT.2020.2984550

Multiple-Input Single-Output Ghost Imaging

Le Wang ¹ and Shengmei Zhao ^{1,2,3}

¹Institute of Signal Processing and Transmission, Nanjing University of Posts and Telecommunications (NUPT), Nanjing 210003, China

²Key Lab of Broadband Wireless Communication and Sensor Network Technology, Nanjing University of Posts and Telecommunications, Ministry of Education, Nanjing 210023, China

³State Key Laboratory of Low-dimensional Quantum Physics, Tsinghua University, Beijing 100084, China

DOI:10.1109/JPHOT.2020.2984550

This work is licensed under a Creative Commons Attribution 4.0 License. For more information, see <https://creativecommons.org/licenses/by/4.0/>

Manuscript received February 28, 2020; revised March 22, 2020; accepted March 27, 2020. Date of publication April 2, 2020; date of current version April 28, 2020. This work was supported in part by the National Natural Science Foundation of China (NSFC) under Grants 61871234 and 11847062, in part by the Natural Science Foundation of Jiangsu Province under Grant BK20180755, in part by Open Research Fund Program of the State Key Laboratory of Low-Dimensional Quantum Physics, Tsinghua University under Grant KF201909, in part by Open research fund of Key Lab of Broadband Wireless Communication and Sensor Network Technology (Nanjing University of Posts and Telecommunications), Ministry of Education (JZNY201910), and in part by NUPTSF (NY218098, NY220004). Corresponding authors: Shengmei Zhao and Le Wang (e-mail: zhaosm@njupt.edu.cn; lewang@njupt.edu.cn).

Abstract: In this paper, we propose a multiple-input single-output ghost imaging scheme, named MISO-GI. In the scheme, K spatiotemporal speckle pattern sources (*multiple input*) simultaneously generate K different spatiotemporal modulated speckle patterns which then are illuminated on an unknown object at the same time. Then, a non-spatial-resolution bucket detector (*single output*) is used to detect the light field interacting with the object. According to the orthogonality of speckle patterns from different spatiotemporal speckle pattern sources, the detection signal is separated into K components corresponding to K spatiotemporal modulated speckle patterns. With the effective recovery algorithm, an image is reconstructed by using all spatiotemporal modulated speckle patterns and their corresponding components of detection signals. Both experimental and simulation results verify the feasibility of the proposed MISO-GI scheme. Moreover, the results also show that the proposed MISO-GI scheme could reduce the total sampling time by K times and improve the imaging quality comparing to traditional GI, without the decrease of the number of speckle patterns and the picture time as well as the consumption of other light field dimensions. It provides a promising avenue to realize GI with limited sampling time and has potential for more applications.

Index Terms: Ghost imaging, multiple-input single-output.

1. Introduction

Ghost imaging (GI) is an intriguing optical imaging technique [1], [2], where the images of objects can be achieved by correlating the fluctuations between the separated optical fields, without the need to record the image itself. GI offers great promise for its higher spatial resolution [3], [4] and higher detection sensitivity [5]. Thus, the past years have witnessed a rapidly growing interest in the applications of GI, ranging from laser radars [6], [7], microscopes [8], [9], object edges extraction [10]–[13], image hiding methods [14]–[16] to optical encryption schemes [17]–[20].

The first GI experiment is realized by exploiting the quantum properties of entangled photon pairs [1]. Then, GI is discussed with classical thermal light or pseudo-thermal light [2], [21]. In conventional thermal GI configuration [3], [21], there are two spatially correlated optical beams. One beam, called signal beam, illuminates on an object and then is detected by a bucket detector without any spatial resolution. The other beam is referred as reference beam, whose light field (speckle pattern) is measured by a spatially resolving detector, such as a CCD or CMOS camera. The imaging is achieved by correlating the two detection signals. Subsequently, computational ghost imaging (CGI) [22] is introduced to simplify the system's configuration, where the light field from reference beam is calculated offline, instead of detection, on the basis of the speckle pattern modulated on the spatial light modulator (SLM) or digital mirror device (DMD).

However, there are still some obstacles in practical implementations of GI. One drawback is that a long sampling time is required for reconstructing a higher quality image because the imaging quality of GI is proportional to the number of speckle patterns and thus the sampling time is required to be long enough to reach a sufficient number of speckle patterns. To overcome this shortage, extra physical dimensions of light field, such as wavelength [23] and polarization [24], are utilized in GI system. By multiplexing other physical dimensions, the sampling time can be reduced. However, it is impossible for these schemes to implement some specific GI applications, such as hyperspectral GI and polarized GI, because these schemes require the consumption of additional physical resources.

Inspired by the concepts of multiple antenna technique [25], including multiple-input-single-output (MISO) technique, in wireless communications, we propose a novel ghost imaging scheme, named multiple-input single-output ghost imaging (MISO-GI), in the paper. In the scheme, K different spatiotemporal modulated speckle patterns are generated simultaneously by K spatiotemporal speckle pattern sources (SSPS) (*multiple input*). Each source is composed by an amplitude modulated source (AM-Source) and a DMD, where the AM-Source generates a light field modulated by a special temporal waveform and the DMD is used to modulate the light field with a spatial distribution. Then, these spatiotemporal modulated speckle patterns are illuminated on an object simultaneously, and the optical intensity interacted with the object is detected by a bucket detector (*single output*). Finally, the image of the object is reconstructed by performing signal processing with the following two steps. (1) By correlation receiving with the special temporal waveform, the signal of bucket detector is separated into K components, corresponding to the spatiotemporal modulated speckle patterns from K SSPSs. (2) A high-quality image is reconstructed by using all spatiotemporal modulated speckle patterns and their corresponding detection signal components.

From the view of object, *multiple* SSPSs sending *multiple* different speckle patterns to illuminate the object resembles the *multiple-input* transmitting antenna in the wireless communications, while *one* bucket detector detecting the light fields from the object likes the *single-output* receiving antenna. Hence, MISO-GI achieves the spatial multiplexing advantages, where it could dramatically reduce the total sampling time (TST) and improve the imaging quality without the decrease of the number of speckle patterns and the picture time as well as the consumption of other physical dimensions of light field. Furthermore, MISO-GI also has the potential to be extended to hyperspectral GI and polarized GI.

The organization of the paper is as follows. In Section 2, MISO-GI is presented. The performance of MISO-GI is discussed by numerical simulations and experiments in Section 3 and Section 4, respectively. Finally, Section 5 concludes the paper.

2. Theory

Fig. 1 shows the schematic diagram of the proposed MISO-GI scheme. There are K SSPSs, each consisting of one DMD and one AM-Source, to generate K spatiotemporal modulated speckle patterns simultaneously. Specifically, the AM-Source in the k th SSPS produces an uniform light field with a special temporal waveform, $\varphi_k(t)$, and the DMD modulates the light to form a spatial speckle pattern, $I_k^i(x, y)$, where (x, y) is Cartesian coordinate and i is the i th speckle pattern. Hence,

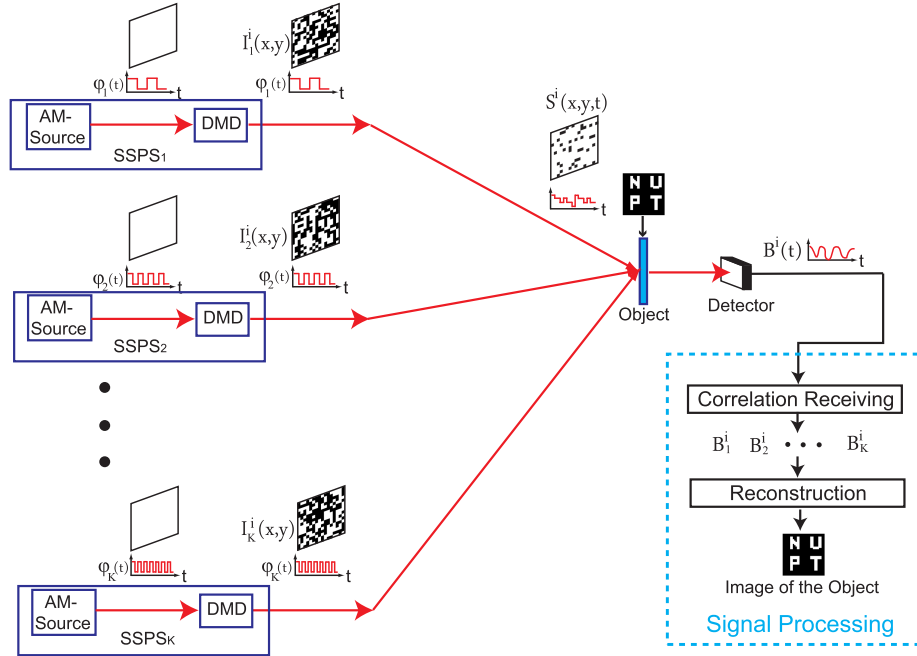


Fig. 1. A schematic diagram of the MISO-GI scheme.

the i th spatiotemporal modulated speckle pattern from k th SSPS is

$$S_k^i(x, y, t) = I_k^i(x, y)\varphi_k(t), \quad (1)$$

where $k = 1, 2, \dots, K$, $i = 1, 2, \dots, M$, K is the number of SSPSs, and M is the number of one set of spatiotemporal modulated speckle patterns. T is the time slot duration of the temporal waveform $\varphi_k(t)$ and $0 < t < T$. Here, the temporal waveform $\varphi_k(t)$ should satisfy

$$\int_0^T \varphi_k(t)\varphi_{k'}(t)dt = \begin{cases} 1, & \text{if } k = k' \\ 0, & \text{else} \end{cases}. \quad (2)$$

Then, K spatiotemporal modulated speckle patterns from K SSPSs are illuminated onto the unknown object simultaneously and are superposed incoherently to form i th superposed spatiotemporal modulated speckle pattern, $S^i(x, y, t)$,

$$S^i(x, y, t) = \sum_{k=1}^K S_k^i(x, y, t). \quad (3)$$

After the interaction with object, the resultant light field is detected by a bucket detector. Hence, the signal of the bucket detector from i th measurement, $B^i(t)$, is

$$B^i(t) = \int_A S^i(x, y, t)O(x, y)dxdy, \quad (4)$$

where $O(x, y)$ is the distribution function of the object. A is the region of the object that reflects or transmits the light into the bucket detector.

Then the component of bucket detection signals corresponding to i th spatiotemporal modulated speckle pattern from k th SSPS, B_k^i , is extracted from $B^i(t)$ by correlation receiving with its special

temporal waveform, $\varphi_k(t)$,

$$\begin{aligned}
 B_k^j &= \int_0^T B^j(t) \varphi_k(t) dt \\
 &= \int_0^T \left(\int_A \sum_{k'=1}^K S_{k'}^j(x, y, t) O(x, y) dx dy \right) \varphi_k(t) dt \\
 &= \sum_{k'=1}^K \int_A I_{k'}^j(x, y) O(x, y) dx dy \int_0^T \varphi_{k'}(t) \varphi_k(t) dt \\
 &= \int_A I_k^j(x, y) O(x, y) dx dy,
 \end{aligned} \tag{5}$$

It is shown that all components of bucket detection signals corresponding to various spatiotemporal modulated speckle pattern can be separated efficiently.

After the detector performs M measurements for M superposed spatiotemporal modulated speckle patterns, $S^j(x, y, t)|_{i=1,2,\dots,M}$, we can obtain MK components of bucket detection signals B_k^j corresponding to MK speckle patterns $I_k^j(x, y)$. Thus the reconstruction algorithms are used to recover the image of the object by using all speckle patterns $I_k^j(x, y)|_{i=1,2,\dots,M}^{k=1,2,\dots,K}$ and corresponding components of bucket detection signals $B_k^j|_{i=1,2,\dots,M}^{k=1,2,\dots,K}$. Here the second-order correlation (2C) algorithm [18] and the fast Walsh-Hadamard transform (FWHT) algorithm [26] are used for the random speckle patterns and Walsh-Hadamard speckle patterns, respectively, where the reconstructed images of the object are

$$\hat{O}_{2C}(x, y) = \frac{1}{MK} \sum_{i=1}^M \sum_{k=1}^K (B_k^i - \overline{B_k^i}) I_k^i(x, y), \tag{6}$$

and

$$\hat{O}_{FWHT}(x, y) = FWHT \left\{ B_k^i |_{i=1,2,\dots,M}^{k=1,2,\dots,K} \right\}, \tag{7}$$

where $\overline{B_k^i} = \frac{1}{MK} \sum_{i=1}^M \sum_{k=1}^K B_k^i$ and $FWHT\{\bullet\}$ represents the FWHT operation with a butterfly computation structure.

Note that the total sampling time (TST) of MISO-GI, $TST^{MISO-GI}$, is determined by the number of measurements M and the picture time T_{pic} , where the picture time T_{pic} is the time of display of speckle patterns and synch processing for DMD. Furthermore, we set T equal to T_{pic} . Therefore, the TST of MISO-GI, $TST^{MISO-GI}$, is

$$TST^{MISO-GI} = M \times T_{pic} = M \times T. \tag{8}$$

However, traditional ghost imaging scheme (TGI) requires sending the speckle patterns from the DMD one after another and performing a measurement for each speckle pattern in turn, so the TST of TGI with M' ($M' = MK$) speckle patterns, TST^{TGI} , is

$$TST^{TGI} = M' \times T_{pic} = MK \times T. \tag{9}$$

It is shown that we can decrease TST^{TGI} by reducing the number of speckle patterns or the picture time T_{pic} . However, the decrease of the number of speckle patterns will deteriorate the imaging quality. On the other hand, the minimum value of picture time T_{pic} is limited by the property of DMD. For example, the existing fastest DMD with high resolution and flexibility has an upper limitation of 22 kHz modulation rate, that is the picture time $T_{pic} \geq 1/22 \text{ kHz} = 45.5 \mu\text{s}$. Additionally, the decrease of picture time T_{pic} will shorten the time of display of speckle patterns for DMD, which resulting in bucket detection signals greatly affected by noise and a lower quality imaging.

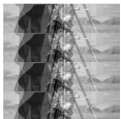
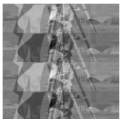
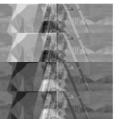
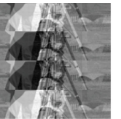


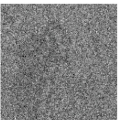
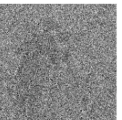
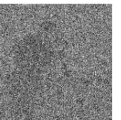


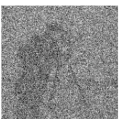
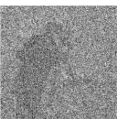
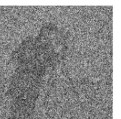

	Image reconstructed by SSPS ₁	Image reconstructed by SSPS ₂	Image reconstructed by SSPS ₃	Image reconstructed by SSPS ₄	Image reconstructed by all SSPSs
Walsh-Hadamard Patterns M=4096 TST=409.6ms	 MSE=0.0501	 MSE=0.0511	 MSE=0.0426	 MSE=0.0489	 MSE=0.00004
Random Patterns M=4096 TST=409.6ms	 MSE=0.0640	 MSE=0.0592	 MSE=0.0609	 MSE=0.0603	 MSE=0.0499
Random Patterns M=10000 TST=1s	 MSE=0.0542	 MSE=0.0554	 MSE=0.0592	 MSE=0.0531	 MSE=0.0432

Fig. 2. The numerical simulations results of the “Cameraman” using MISO-GI schemes with four SSPSs ($K = 4$).

Hence, the TST can be reduced by K times by using MISO-GI comparing to TGI without the decrease of the number of speckle patterns and the picture time as well as the consumption of other physical dimensions of light field.

3. Numerical Simulations

In this section, we discuss the performance of the proposed MISO-GI scheme by numerical simulations. In order to compare the quality of the reconstructed image quantitatively, mean square error (MSE) is used as an objective evaluation, which is defined as

$$MSE = \frac{1}{N} \sum_{x,y} (\hat{O}(x,y) - O(x,y))^2, \quad (10)$$

where $O(x,y)$ and $\hat{O}(x,y)$ denote the intensity values of the original image and the reconstructed image, respectively. N is number of pixels of the image.

To verify the feasibility of MISO-GI scheme, the numerical simulations are performed and the results are shown in Fig. 2. Here we use four SSPSs ($K = 4$) in the MISO-GI system, and the temporal waveforms $\varphi_k(t)$ for four SSPSs are sine waves with the frequency 110 kHz, 130 kHz, 150 kHz, and 170 kHz. Both binary random and Walsh-Hadamard speckle patterns with 128×128 -pixels are used to illuminate onto the object, where the i th Walsh-Hadamard speckle pattern is obtained by reshaping the i th row of the natural order Walsh-Hadamard transform matrix (the number of rows of the natural order Walsh-Hadamard transform matrix is N) [26] and four SSPSs generate Walsh-Hadamard patterns from first, second, third and last quarter of rows of the natural order Walsh-Hadamard transform matrix, respectively. Simultaneously, the picture time is set up as $T_{pic} = 100 \mu s$ and the sampling rate of the analogue-to-digital converter is setup as 1 MS/s. The results of the first row in Fig. 2 are obtained by using Walsh-Hadamard patterns, while results of the second and third row in Fig. 2 are obtained by using binary random patterns. Additionally, the results of the first to fourth column in Fig. 2 are obtained by using the components of bucket detection signals corresponding to the spatiotemporal modulated speckle patterns from SSPS₁ to SSPS₄, respectively. These components of bucket detection signals are extracted from the bucket detection signal by correlation receiving with special temporal waveform $\varphi_k(t)$ ($k = 1, 2, 3, 4$). Then

Scheme Resolution	MISO-GI K=2	MISO-GI K=4	MISO-GI K=8	TGI
32 × 32	 MSE=0.01617 TST=51.2ms	 MSE=0.01617 TST=25.6ms	 MSE=0.01617 TST=12.8ms	 MSE=0.01617 TST=102.4ms
64 × 64	 MSE=0.00064 TST=204.8ms	 MSE=0.00064 TST=102.4ms	 MSE=0.00064 TST=51.2ms	 MSE=0.00064 TST=409.6ms
128 × 128	 MSE=0.00004 TST=819.2ms	 MSE=0.00004 TST=409.6ms	 MSE=0.00004 TST=204.8ms	 MSE=0.00004 TST=1.6384s

Fig. 3. The numerical simulations results of the “Cameraman” using MISO-GI schemes with different number of SSPSs and TGI scheme by using Walsh-Hadamard patterns, where both MSE and TST are presented.

the full image of the object is recovered by using all spatiotemporal modulated speckle patterns from all SSPSs and their corresponding components of bucket detection signals and the results are shown in the last column of Fig. 2. The results show that we cannot reconstruct a clear image when we only use the detection signals B_k^j corresponding to the spatiotemporal modulated Walsh-Hadamard speckle patterns from SSPS₁, SSPS₂, SSPS₃, or SSPS₄, because only one quarter of the complete set of Walsh-Hadamard speckle patterns are used. However, a clear image is able to obtain when a complete set of Walsh-Hadamard speckle patterns and their corresponding components of detection signals $B_k^j|_{k=1,2,3,4}$ from all SSPSs are used. Moreover, the results in the second and third row of Fig. 2 show that the full image can be obtained by using the detection signals corresponding to the patterns from all SSPSs, where the imaging quality is better and corresponding MSE is smaller than the results that reconstructed by using the detection signals corresponding to the patterns from only one SSPS when the TST is the same.

Furthermore, to verify that MISO-GI scheme has the ability to reduce TST by K times for the reconstruction of the image of the object comparing to TGI without the decrease of the number of speckle patterns and the picture time, the numerical simulations are performed and the results are shown in Fig. 3. Here we use Walsh-Hadamard speckle patterns with 32×32 -pixels, 64×64 -pixels, and 128×128 -pixels, respectively. Simultaneously, we respectively use MISO-GI schemes with two SSPSs ($K = 2$ and the corresponding $\varphi_k(t)$ are sine waves with the frequency 110 kHz and 150 kHz), four SSPSs ($K = 4$ and the corresponding $\varphi_k(t)$ are sine waves with the frequency 110 kHz, 130 kHz, 150 kHz, and 170 kHz), and eight SSPSs ($K = 8$ and the corresponding $\varphi_k(t)$ are sine waves with the frequency 110 kHz, 130 kHz, 150 kHz, 170 kHz, 190 kHz, 210 kHz, 230 kHz, and 250 kHz) and TGI scheme to do the numerical simulation. The picture time is set up as $T_{pic} = 100 \mu\text{s}$ and the sampling rate is setup as 1 MS/s. All images are recovered by using a complete set of Walsh-Hadamard speckle patterns. Due to the number of speckle patterns and the picture time are the same for all schemes, both the quality and the MSE of reconstructed images are the same. However, TST of MISO-GI scheme with K SSPSs is $1/K$ of that of TGI because MISO-GI scheme with K SSPSs can generate and illuminate K different speckle patterns simultaneously.

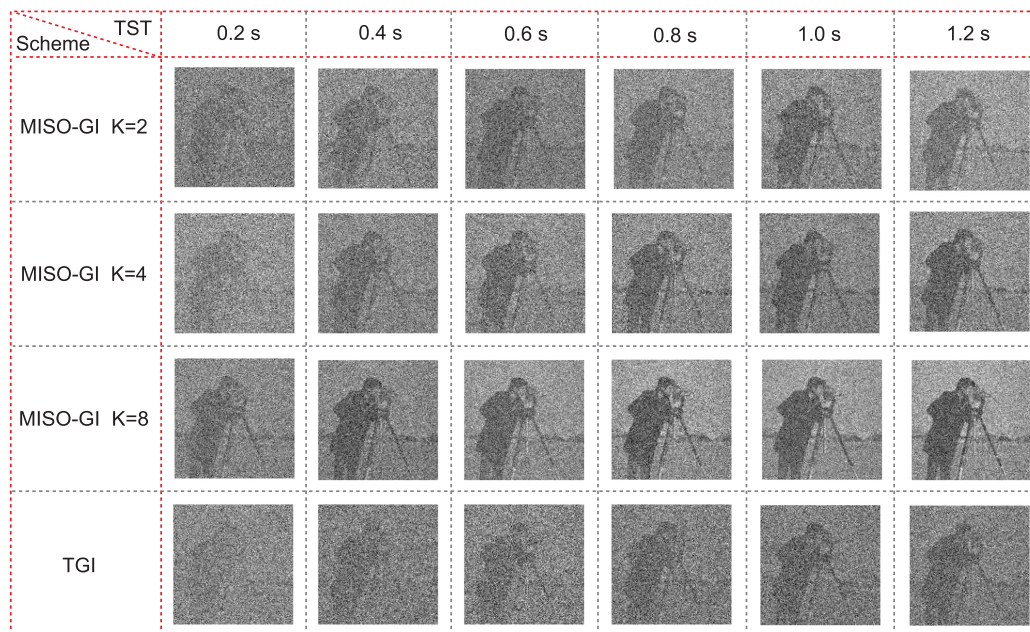


Fig. 4. The numerical simulations results of the “Cameraman” using MISO-GI schemes with different number of SSPSs and TGI scheme by using binary random patterns.

Moreover, we consider that the imaging quality and MSE of reconstructed images are influenced by MISO-GI schemes with different number of SSPSs and TGI scheme by using binary random patterns under the same condition of TST and the picture time. The reconstructed images from one realization are shown in Fig. 4 and then the MSEs are the average of 20 simulated results as a function of TST shown in Fig. 5. Here we use binary random speckle patterns with 128×128 -pixels, and we respectively use MISO-GI schemes with two SSPSs ($K = 2$), four SSPSs ($K = 4$), and eight SSPSs ($K = 8$) and TGI scheme, where the corresponding $\varphi_k(t)$ are the same as those of Fig. 3. The picture time and the sampling rate are set up as $T_{pic} = 100 \mu\text{s}$ and 1 MS/s , respectively. It is found that the imaging quality of reconstructed images of MISO-GI schemes is better than that of TGI and corresponding MSEs are smaller. In addition, the quality of reconstructed images of MISO-GI schemes improves and corresponding MSEs decrease gradually with the increase of K when TST is the same, because the number of speckle patterns of MISO-GI scheme with K SSPSs is K times of that of TGI under the same condition of TST.

4. Experiments

In this section, we discuss the performance of the proposed scheme by experiments.

The experimental system of the MISO-GI scheme with two SSPSs ($K = 2$) is shown in Fig. 6. Two red LEDs (LED_1 and LED_2) are driven by a Arbitrary Waveform Generator (Keysight 33612 A) with special temporal waveform $\varphi_1(t)$ and $\varphi_2(t)$, where $\varphi_1(t)$ and $\varphi_2(t)$ are the sine waves with the frequency 100 kHz and 160 kHz, respectively, while both of them have the same amplitude $3V_{pp}$ and DC offset 3 V. Both DMD₁ and DMD₂ (ViALUX V-7001) are controlled by a computer to modulate the light from LED_1 and LED_2 to generate two sets of the spatiotemporal modulated speckle patterns, $S_1^i(x, y, t)$ and $S_2^i(x, y, t)$, respectively. Then two sets of the spatiotemporal modulated speckle pattern pairs, $S_1^i(x, y, t)$ and $S_2^i(x, y, t)$, have the same size and are superposed incoherently by adjusting the mirrors and then are formed as the superposed spatiotemporal modulated speckle pattern, $S^i(x, y, t)$, by using a beam splitter (BS). Then the superposed spatiotemporal modulated speckle pattern, $S^i(x, y, t)$, is illuminated onto an object, where we use a USAF resolution chart as

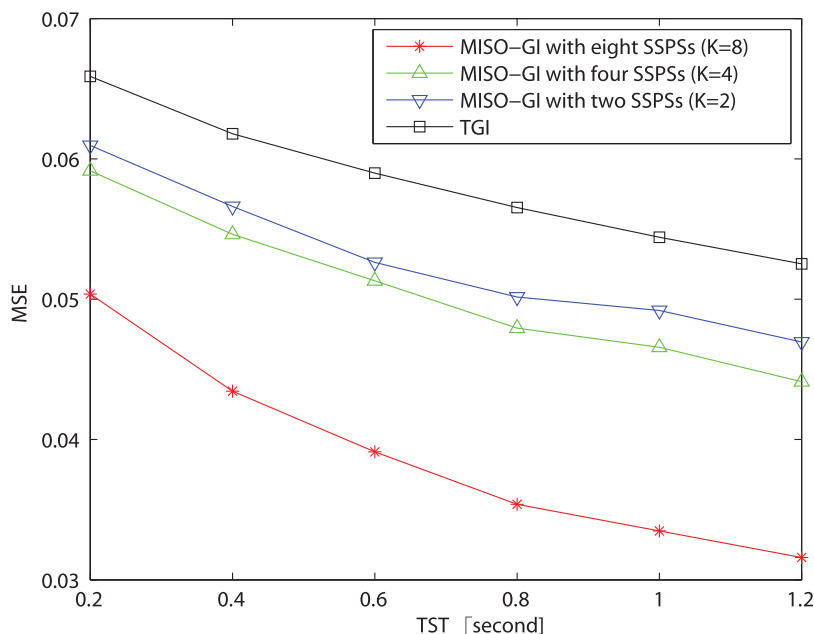


Fig. 5. The numerical simulation results of reconstructed “Cameraman” images’ MSEs as a function of TST for MISO-GI schemes with different number of SSPs and TGI scheme by using binary random patterns.

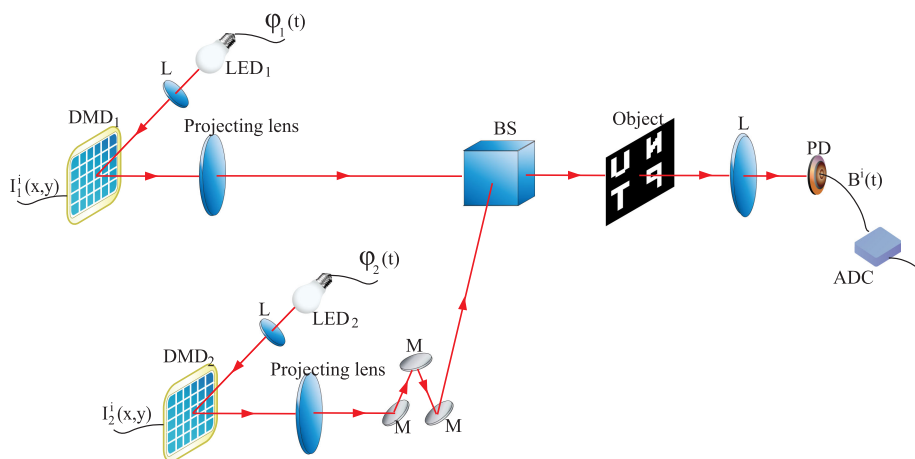


Fig. 6. An experimental setup for the MISO-GI scheme system. LED: Light emitting diode. DMD: Digital mirror device. L: Lens. M: Mirror. BS: Beam splitter. PD: Photodetector. ADC: Analog-to-digital converter.

the object. In addition, to ensure that two DMDs generate speckle patterns at the same time we make two DMDs work at the slave mode and driven by a square wave with the frequency 20 kHz, amplitude 1.4 Vpp, DC offset 700 mV and duty ratio 50% from another Arbitrary Waveform Generator. The transmitting light is detected by a photodetector (Thorlabs PDA100A-EC with 40 dB gain) after a lens and then a computer records detection results $B^i(t)$ via an analogue-to-digital converter (NI USB-6351) whose sampling rate is setup as 1 MS/s. Finally, the component of bucket detection signals B_1^i and B_2^i can be extracted from $B^i(t)$ and then the images of the object are reconstructed by using all modulated speckle patterns $I_k^i(x, y)|_{i=1,2,\dots,M}^{k=1,2}$ and corresponding component of bucket detection signals $B_k^i|_{i=1,2,\dots,M}^{k=1,2}$.

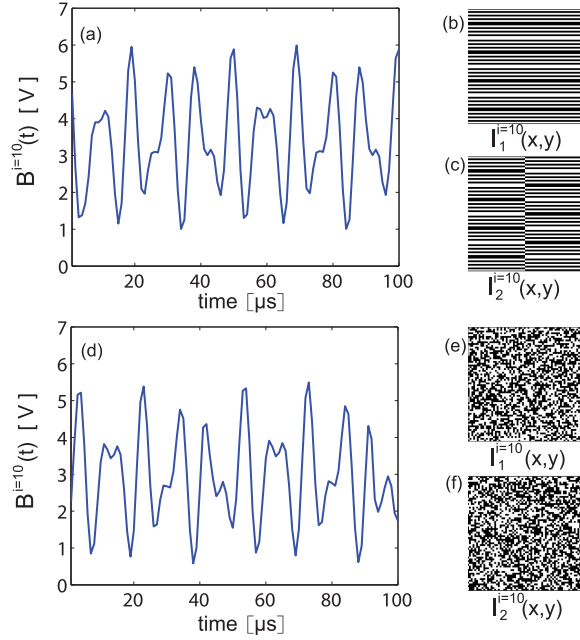


Fig. 7. (a) is the detection result for the tenth spatiotemporal modulated Walsh-Hadamard speckle pattern, $B^{i=10}(t)$. (b) is the tenth Walsh-Hadamard speckle pattern modulated by DMD₁, $I_1^{i=10}(x, y)$. (c) is the tenth Walsh-Hadamard speckle pattern modulated by DMD₂, $I_2^{i=10}(x, y)$. (d) is the detection result for the tenth spatiotemporal modulated random speckle pattern, $B^{i=10}(t)$. (e) is the tenth binary random speckle pattern modulated by DMD₁, $I_1^{i=10}(x, y)$. (f) is the tenth binary random speckle pattern modulated by DMD₂, $I_2^{i=10}(x, y)$.

We perform the experiment to verify the feasibility of MISO-GI scheme. Here we use two SSPSs ($K = 2$) in the experiment, and both binary random and Walsh-Hadamard speckle patterns are 64×64 -pixels, where DMD₁ and DMD₂ generate Walsh-Hadamard patterns from first and last half of rows of the natural order Walsh-Hadamard transform matrix, respectively. Additionally, the picture time is set up as $T_{pic} = 100 \mu\text{s}$. In the experiment, Fig. 7(a) and (d) are the detection results $B^i(t)$ for the tenth spatiotemporal modulated Walsh-Hadamard and binary random speckle patterns, respectively, both of which are sampled by the ADC. In addition, we show the tenth Walsh-Hadamard speckle patterns modulated by DMD₁ and DMD₂ in Fig. 7(b) and (c), respectively. Fig. 7(e) and (f) are the tenth binary random speckle patterns modulated by DMD₁ and DMD₂, respectively. By computing Eq. (5) with the temporal waveform $\varphi_1(t)$ and $\varphi_2(t)$, we can extract the components of bucket detection signals B_1^i and B_2^i from $B^i(t)$. Therefore, we can obtain $B_1^{i=10} = 78.3914$ and $B_2^{i=10} = 49.9920$ from Fig. 7(a) and $B_1^{i=10} = 67.0875$ and $B_2^{i=10} = 53.8165$ from Fig. 7(d).

Fig. 8 shows the experimental results, where the results of the first and second row in Fig. 8 are obtained by using Walsh-Hadamard patterns and binary random patterns, respectively. In addition, the first and second column in Fig. 8 show the results obtained by using the components of bucket detection signals corresponding to the spatiotemporal modulated speckle patterns from SSPS₁ and SSPS₂, respectively. Then the last column of Fig. 8 shows the results recovered by using all spatiotemporal modulated speckle patterns from all SSPSs and their corresponding components of bucket detection signals. It is shown that a clear image cannot be reconstructed when we only use the detection signals B_k^i corresponding to the spatiotemporal modulated Walsh-Hadamard speckle patterns from SSPS₁ or SSPS₂, because only one half of the complete set of Walsh-Hadamard speckle patterns are used. However, we can obtain a clear image when both a complete set of Walsh-Hadamard speckle patterns and their corresponding components of detection signals $B_k^i|_{k=1,2}$ from all SSPSs are used. Moreover, by using the detection signals corresponding to the

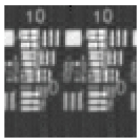
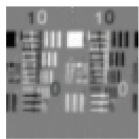
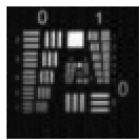



	Image reconstructed by SSPS ₁	Image reconstructed by SSPS ₂	Image reconstructed by all SSPS _s
Walsh-Hadamard Patterns M=2048 TST=204.8ms	 MSE=0.2596	 MSE=0.3799	 MSE=0.1078
Random Patterns M=20000 TST=2s	 MSE=0.2051	 MSE=0.2581	 MSE=0.1868

Fig. 8. The experimental results of the resolution chart using MISO-GI scheme with two SSPSs ($K = 2$).

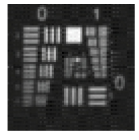
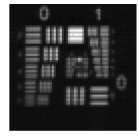
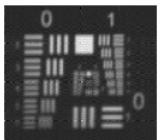
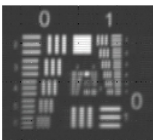
Scheme: Resolution	MISO-GI $K=2$ $T_{pic}=50\mu s$	TGI $T_{pic}=50\mu s$
64×64	 MSE=0.1478 TST=102.4ms	 MSE=0.1350 TST=204.8ms
128×128	 MSE=0.1597 TST=409.6ms	 MSE=0.1881 TST=819.2ms

Fig. 9. The experimental results of the resolution chart using MISO-GI scheme with two SSPSs ($K = 2$) and TGI scheme by using Walsh-Hadamard speckle patterns under the same condition of the number of speckle patterns and the picture time.

binary random patterns from all SSPSs, the image of object can be reconstructed and shown in the lower right corner of Fig. 8, where the imaging quality is better and corresponding MSE is smaller than the results that reconstructed by using the detection signals corresponding to the patterns from only one SSPS.

Furthermore, we do the experiment to verify that MISO-GI scheme has the ability to reduce TST by K times for the reconstruction of the image of the object comparing to TGI under the same condition of the number of speckle patterns and the picture time, where the results are shown in Fig. 9. Here we use Walsh-Hadamard speckle patterns with 64×64 -pixels and 128×128 -pixels, respectively and all of results are recovered by using a complete set of Walsh-Hadamard speckle patterns. Simultaneously, we set up the picture times as $T_{pic} = 50 \mu s$. The results show that when we use the same number of speckle patterns and the same picture time, we can obtain a clear image by using MISO-GI and TGI scheme, whose imaging quality and MSEs are close. However, TST of MISO-GI scheme is half of that of TGI because MISO-GI scheme with two SSPSs can generate and illuminate two different speckle patterns simultaneously.

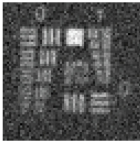
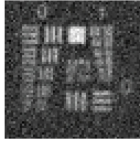

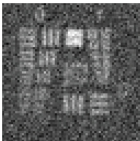
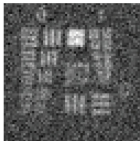

Scheme	TST	0.5 s	1 s	2 s
MISO-GI $K=2$				
	MSE=0.2150 $T_{pic}=50\mu s$ $M=10000$	MSE=0.2057 $T_{pic}=100\mu s$ $M=10000$	MSE=0.1868 $T_{pic}=100\mu s$ $M=20000$	
				
TGI	MSE=0.2593 $T_{pic}=50\mu s$ $M'=10000$	MSE=0.2480 $T_{pic}=100\mu s$ $M'=10000$	MSE=0.2030 $T_{pic}=100\mu s$ $M'=20000$	

Fig. 10. The experimental results of the resolution chart using MISO-GI scheme with two SSPSs ($K = 2$) and TGI scheme by using binary random speckle patterns under the same condition of TST and the picture time. For each column, the number of speckle patterns of MISO-GI is twice than that of TGI.



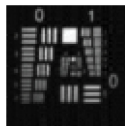
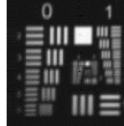

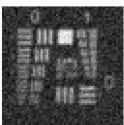
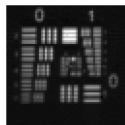
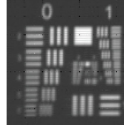
Scheme	TST	1 s	2 s	204.8ms	819.2ms
MISO-GI $K=2$ $T_{pic}=100\mu s$					
	MSE=0.2057	MSE=0.1868	MSE=0.1078	MSE=0.1190	
TGI $T_{pic}=50\mu s$					
	MSE=0.2185	MSE=0.1871	MSE=0.1350	MSE=0.1881	

Fig. 11. The experimental results of the resolution chart using MISO-GI scheme with two SSPSs ($K = 2$) and TGI scheme by using Walsh-Hadamard and binary random speckle patterns under the same condition of TST and the number of speckle patterns.

Moreover, Fig. 10 compares the images reconstructed by MISO-GI to those of TGI experimentally under the same condition of TST and the picture time. Here we use binary random speckle patterns with 64×64 -pixels. We find that the imaging quality of reconstructed images of MISO-GI schemes is better than that of TGI and corresponding MSEs are smaller, because the number of speckle patterns used in the MISO-GI scheme is twice as much as that of TGI at the same TST. In addition, by comparing the first and second column in Fig. 10 for both MISO-GI and TGI scheme, we can find that the imaging quality will be better and corresponding MSEs will decrease when the picture time is prolonged under the same condition of the number of speckle patterns. Furthermore, the images will be more clear and corresponding MSEs will decrease with the increase of the number of speckle patterns under the same condition of picture time for both MISO-GI and TGI scheme by comparison of the second and third column in Fig. 10.

Lastly, Fig. 11 shows the experimental results to verify that MISO-GI can improve the imaging quality comparing to TGI under the same condition of TST and the number of speckle patterns. The results of the first and second column in Fig. 11 are obtained by using binary random speckle

patterns with 64×64 -pixels, while Walsh-Hadamard speckle patterns with 64×64 -pixels and 128×128 -pixels are used to reconstruct the images shown in the third and last column of Fig. 11, respectively. The number of speckle patterns used to reconstruct the images shown in the first and second column of Fig. 11 are 20000 and 40000, respectively. The images shown in the third and last column of Fig. 11 are recovered by using a complete set of Walsh-Hadamard speckle patterns. Because we shorten the picture time of TGI by half of that of MISO-GI, TSTs of both MISO-GI and TGI are the same. The results of Fig. 11 show the MISO-GI can improve the imaging quality and acquire the smaller MSEs comparing to TGI for both Walsh-Hadamard and binary random speckle patterns, because with the comparison of TGI, MISO-GI has a longer picture time and thus MISO-GI has a better ability to resist the impact of noise which resulting in the improvement of the imaging quality.

5. Conclusion

We have proposed a novel ghost imaging scheme, named multiple-input single-output ghost imaging (MISO-GI) in the paper. In the scheme, *multiple* spatiotemporal modulated speckle patterns have been generated simultaneously by *multiple* SSPSs, representing *multiple input*, and a bucket detector has been utilized to detect their incident light fields after interacting with the object individually (*single output*). With the designed steps, the image of the object has been reconstructed by all spatiotemporal modulated speckle patterns and their corresponding component of bucket detection signals. The experimental and numerical results have shown that the proposed MISO-GI scheme has dramatically reduced TST and improved the imaging quality without the decrease of the number of speckle patterns and the picture time as well as the consumption of other physical dimensions of light field. MISO-GI will become a promising scheme for high-speed GI and has the potential to be extended to hyperspectral GI and polarized GI. In addition, compressed sensing [27] algorithm has been used in GI schemes [28]–[31] to reconstruct a high quality image of object and to reduce both the TST and the number of speckle patterns significantly by the aid of the redundant structure of the images. Hence, the 2C algorithm and the FWHT algorithm can be replaced by compressed sensing algorithm in the MISO-GI scheme to further reduce the TST.

References

- [1] D. V. Strelakov, A. V. Sergienko, D. N. Klyshko, and Y. H. Shih, "Observation of two-photon "ghost" interference and diffraction," *Phys. Rev. Lett.*, vol. 74, no. 18, pp. 3600–3603, 1995.
- [2] R. S. Bennink, S. J. Bentley, and R. W. Boyd, "'Two-photon' coincidence imaging with a classical source," *Phys. Rev. Lett.*, vol. 89, no. 11, pp. 113601–113604, 2002.
- [3] D. Z. Cao, G. J. Ge, and K. Wang, "Two-photon subwavelength lithography with thermal light," *Appl. Phys. Lett.*, vol. 97, no. 5, 2010, Art. no. 051105.
- [4] W. Gong and S. Han, "Experimental investigation of the quality of lensless super-resolution ghost imaging via sparsity constraints," *Phys. Lett. A*, vol. 376, no. 17, pp. 1519–1522, 2012.
- [5] W. T. Liu, "Discussions on advantages of ghost imaging compared to traditional optical imaging," in *Proc. Frontiers Opt.*, 2016, Paper JW4A.56.
- [6] G. A. Howland, P. B. Dixon, and J. C. Howell, "Photon-counting compressive sensing laser radar for 3D imaging," *Appl. Opt.*, vol. 50, no. 31, pp. 5917–5920, 2011.
- [7] C. Deng, W. Gong, and S. Han, "Pulse-compression ghost imaging lidar via coherent detection," *Opt. Express*, vol. 24, no. 23, pp. 25983–25994, 2016.
- [8] N. Radwell, K. J. Mitchell, G. M. Gibson, M. P. Edgar, R. Bowman, and M. J. Padgett, "Single-pixel infrared and visible microscope," *Optica*, vol. 1, no. 5, pp. 285–289, 2014.
- [9] N. Tian, Q. Guo, A. Wang, D. Xu, and L. Fu, "Fluorescence ghost imaging with pseudothermal light," *Opt. Lett.*, vol. 36, no. 16, pp. 3302–3304, 2011.
- [10] X. F. Liu, X. R. Yao, R. M. Lan, C. Wang, and G. J. Zhai, "Edge detection based on gradient ghost imaging," *Opt. Express*, vol. 23, no. 26, pp. 33802–33811, 2015.
- [11] L. Wang, L. Zou, and S. M. Zhao, "Edge detection based on subpixel-speckle-shifting ghost imaging," *Opt. Commun.*, vol. 407, pp. 181–185, 2018.
- [12] H. Ren, S. M. Zhao, J. Gruska, "Edge detection based on single-pixel imaging," *Opt. Express*, vol. 26, no. 5, pp. 5501–5511, 2018.
- [13] T. Mao, Q. Chen, W. He, Y. Zou, H. Dai, and G. Gu, "Speckle-shifting ghost imaging," *IEEE Photon. J.*, vol. 8, no. 4, 2016, Art. no. 6900810.

- [14] L. Wang, S. M. Zhao, W. Cheng, L. Gong, and H. Chen, "Optical image hiding based on computational ghost imaging," *Opt. Commun.*, vol. 366, pp. 314–320, 2016.
- [15] W. Chen, and X. Chen, "Marked ghost imaging," *Appl. Phys. Lett.*, vol. 104, no. 25, 2014, Art. no. 251109.
- [16] S. Jiao, C. Zhou, Y. Shi, W. Zou, and X. Li, "Review on optical image hiding and watermarking techniques," *Opt. Laser Technol.*, vol. 109, pp. 370–380, 2019.
- [17] P. Clemente, V. Durán, V. Torres-Company, E. Tajahuerce, and J. Lancis, "Optical encryption based on computational ghost imaging," *Opt. Lett.*, vol. 35, no. 14, pp. 2391–2393, 2010.
- [18] S. M. Zhao, L. Wang, W. Liang, W. Cheng, and L. Gong, "High performance optical encryption based on computational ghost imaging with QR code and compressive sensing technique," *Opt. Commun.*, vol. 353, pp. 90–95, 2015.
- [19] M. Tanha, R. Kheradmand, and S. Ahmadi-Kandjani, "Gray-scale and color optical encryption based on computational ghost imaging," *Appl. Phys. Lett.*, vol. 101, no. 10, 2012, Art. no. 101108.
- [20] X. Huang, Y. Bai, and X. Fu, "Stable and secure image transmission based on temporal ghost imaging," *J. Opt.*, vol. 21, no. 5, 2019, Art. no. 055701.
- [21] X. F. Liu, X. H. Chen, X. R. Yao, W. K. Yu, G. J. Zhai, and L. A. Wu, "Lensless ghost imaging with sunlight," *Opt. Lett.*, vol. 39, no. 8, pp. 2314–2317, 2014.
- [22] J. H. Shapiro, "Computational ghost imaging," *Phys. Rev. A*, vol. 78, no. 6, 2008, Art. no. 061802(R).
- [23] D. J. Zhang *et al.*, "Wavelength-multiplexing ghost imaging," *Phys. Rev. A*, vol. 92, no. 1, 2015, Art. no. 013823.
- [24] S. Dongfeng *et al.*, "Polarization-multiplexing ghost imaging," *Opt. Lasers Eng.*, vol. 102, pp. 100–105, 2018.
- [25] A. Goldsmith, *Wireless Communications*. Cambridge, U.K.: Cambridge Univ. Press, 2005.
- [26] L. Wang and S. Zhao, "Fast reconstructed and high-quality ghost imaging with fast Walsh-Hadamard transform," *Photonics Research*, vol. 4, no. 6, pp. 240–244, 2016.
- [27] A. Stern, *Optical Compressive Imaging*. Boca Raton, FL, USA: CRC Press, 2016.
- [28] O. Katz, Y. Bromberg, and Y. Silberberg, "Compressive ghost imaging," *Appl. Phys. Lett.*, vol. 95, 2009, Art. no. 131110.
- [29] L. Wang and S. Zhao, "Compressed ghost imaging based on differential speckle patterns," *Chin. Phys. B*, vol. 29, 2020, Art. no. 024204.
- [30] F. Soldevila *et al.*, "Single-pixel polarimetric imaging spectrometer by compressive sensing," *Appl. Phys. B*, vol. 113, pp. 551–558, 2013.
- [31] V. Kravets, P. Kondrashov, and A. Stern, "Compressive ultraspectral imaging using multiscale structured illumination," *Appl. Opt.*, vol. 58, pp. F32–F39, 2019.